

# Indentation based strength analysis of adhesively bonded leading-edge composite joints in wind turbine blades.

DROUBI, M.G., FOSBROOKE, C., MCCONNACHIE, J., FAISAL, N.H.


2019





Research Article

# Indentation based strength analysis of adhesively bonded leading-edge composite joints in wind turbine blades

M. G. Droubi<sup>1</sup>  · C. Fosbrooke<sup>1</sup> · J. McConnachie<sup>1</sup> · N. H. Faisal<sup>1</sup>

© The Author(s) 2019 [OPEN](#)

## Abstract

Wind turbine is a source of non-polluting renewable energy. Whether a wind turbine is viable depends entirely on the structural integrity of turbine blade. To assess the structural integrity of wind turbine blades it is necessary to investigate the loading behaviour of adhesively bonded composite joints. Finite element along with cohesive zone modelling (CZM) methods were implemented to investigate the elastic indentation contact of adhesively bonded leading-edge composite joints in wind turbine blades. The CZM was validated by replicating existing experimental and numerical work on composite-to-adhesive bonds applied to wind turbine structures. This validated model was then used to investigate the structural integrity of a variety of leading-edge joint configurations, adhesive thicknesses and bond finishes under indentation. Numerical results showed that an off-centre adhesive joint configuration was desirable and capable of withstanding between 39 and 96% more load than centred joints. Direct indenter to adhesive contact was shown to reduce fracture resistance by up to 4.7%. An adhesive joint based on a lap joint configuration was proposed as an alternative to current designs.

**Keywords** Wind turbine blade · Adhesive joints · Stress analysis · Finite element method · Indentation

## Abbreviations

CFRP Carbon fibre reinforced polymers  
CZM Cohesive zone model  
DCB Double cantilever beam  
ENF End-notch flexure  
FE Finite element  
GFRP Glass fibre reinforced polymers  
VCCT Virtual crack closure technique

$K_C$  Stress intensity factor (fracture toughness)  
 $m$  Mass  
 $s$  Slow down distance  
 $v$  Velocity  
 $\sigma^n$  Normal stress component in the adhesive material  
 $\sigma^t$  Tangential stress component in the adhesive material  
 $\sigma^s$  Shear stress component in the adhesive material  
 $\sigma_{max}^n$  Maximum normal stress component in the adhesive material  
 $\sigma_{max}^t$  Maximum tangential stress component in the adhesive material  
 $\sigma_{max}^s$  Maximum shear stress component in the adhesive material

## List of symbols

$E$  Elastic modulus  
 $F_s$  Slow down force  
 $G_C$  Critical fracture energy release rate  
 $G_{IC}$  Critical fracture energy release rate (Mode I)  
 $G_{IIc}$  Critical fracture energy release rate (Mode II)  
 $G_{IIIc}$  Critical fracture energy release rate (Mode III)  
 $G_I$  Fracture energy release rate (Mode I)  
 $G_{II}$  Fracture energy release rate (Mode II)  
 $G_{III}$  Fracture energy release rate (Mode III)

✉ M. G. Droubi, m.g.droubi@rgu.ac.uk; N. H. Faisal, n.h.faisal@rgu.ac.uk | <sup>1</sup>School of Engineering, Robert Gordon University, Garthdee Road, Aberdeen AB10 7GJ, UK.



SN Applied Sciences (2019) 1:691

| <https://doi.org/10.1007/s42452-019-0735-6>

Received: 14 March 2019 / Accepted: 4 June 2019

Published online: 10 June 2019

SN Applied Sciences  
A **SPRINGER NATURE** journal

## 1 Introduction

Predicting failures in turbine blade composite lay-ups or adhesive joints is a key aspect in assessing their structural integrity, for a reliable renewable energy production. Adhesives are fundamental to modern-day wind turbine blade structures, favoured due to their high strength to weight ratio and flexible nature. Adhesive failure and the occurrence of de-bonding within a wind turbine blade is highlighted as one of the main causes of damage, particularly with the development of larger blades [1]. Materials used in modern wind turbine blade construction are fibre-reinforced polymers due to their good fatigue properties, high specific stiffness, ability to be tailored by differing fibre lay-up orientations and low density. Glass fibre reinforced polymers (GFRP) are the most commonly used composites. Carbon fibre reinforced polymers (CFRP) are occasionally used but limited to local reinforcement only due to their high cost. There are many adhesive joints throughout a turbine blade's internal structure as shown in Fig. 1a. However, the focus of this study is the leading-edge adhesive joint as this is the most likely area to be exposed to indentation or impact loading. Several recognised adhesive joint configurations exist, with a summary of the main ones shown in Fig. 1b.

A fracture mechanics approach is an effective method of determining damage and energy release rates during adhesive failure, and was implemented by Feraren et al. [2], Ji et al. [3] and Floros et al. [4]. However, such an approach becomes invalid if the fracture consists of a crack tip and large non-linear zone. The finite element (FE) method, combined with a simulation technique known as a cohesive zone model (CZM), provides an effective means of analysing adhesive failure in bonded joints. Hazimeh et al. [5] used these to analyse adhesively bonded composite double lap joints subjected to in-plane dynamic impact loads. Floros et al. [4] used an experimental procedure and the numerical simulation to investigate Mode-I, Mode-II and mixed mode (I and II) fracture characteristics of adhesively bonded composite joints. This involved a double cantilever beam (DCB) for Mode-I, and end-notch flexure (ENF) for Mode-II experiments, as well as corresponding FE models. Their results concluded that the FE/CZM and experimental validation method worked well in Mode-I cases, but in Mode-II and mixed mode cases, modifications to the CZM parameters were needed to obtain satisfactory results. Similar procedures of experimental CZM validation were implemented by Prathuru et al. [6]. These studies highlighted the usefulness of these methods but they are not specifically applied to the composite to adhesive bonds found in wind turbine applications.

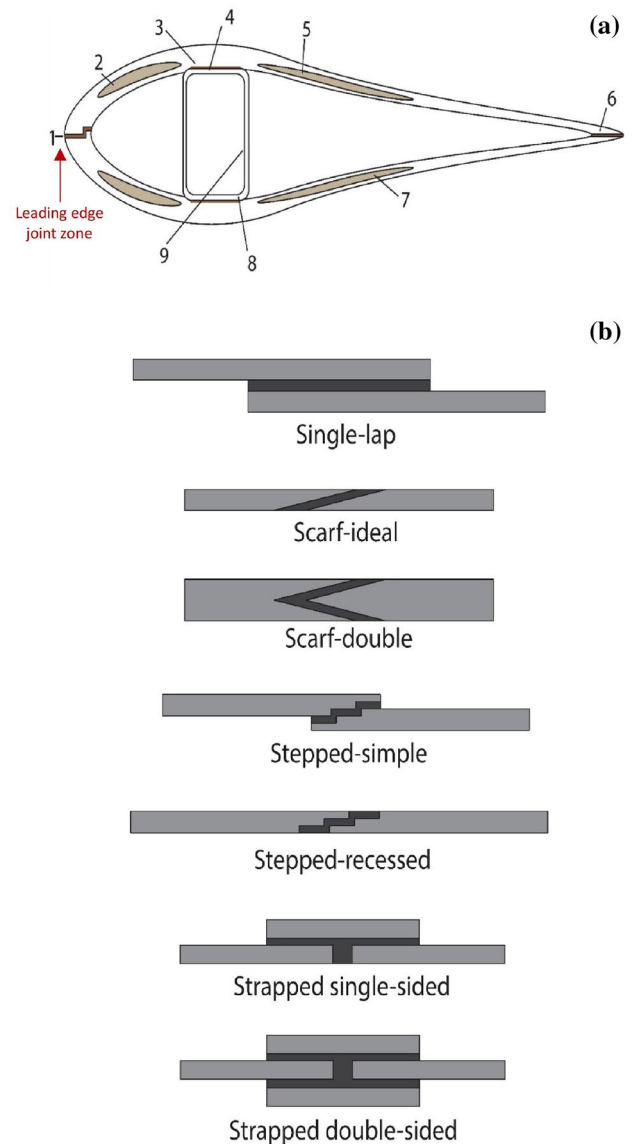


**Fig. 1** Adhesive bond joints: **a** commonly found turbine blade structure, showing single rectangular spar [where, (1) leading edge adhesive joint, (2) aerodynamic panels made as a sandwich structure with foam or wood cores, (3) adhesive joint (suction side), (4) suction side spar cap, (5) suction side mould, (6) trailing edge adhesive joint, (7) pressure side mould, and (8) pressure side spar cap, and **b** common adhesive joint configurations widely applied in various applications

Petterson [7] carried out the design and analysis of a wind turbine adhesive joint using the FE method and a CZM to investigate the adhesive strength of a carbon fibre box spar joint under extreme tensile loads. Using this, he optimised the design of the adhesive joint configuration by analysing the stress concentrations around the bond interfaces. Eder et al. [8] highlighted and investigated the use of the virtual crack closure technique (VCCT), an alternative theory to CZM, and the effect of geometric

non-linearity on energy release rates of adhesive cracks under bi-axial bending in a realistic wind turbine blade cross section. They concluded that taking a simplified cross-sectional slice of complex turbine blade leading edge geometries was an effective method for analysing structures with geometric non-linearity.

Hua et al. [9] investigated the performance of carbon/epoxy composite to adhesive bonds in wind turbine blades subjected to combined bending and torsional loading by using the FE method and a traction–separation law to predict crack initiation and propagation. They showed that non-filletted adhesive finishes and internal adhesive defects caused significant reduction in adhesive bond strength due to increased stress concentrations. Zarouchas et al. [10] implemented a CZM to investigate 4-point bending of an adhesively bonded composite I-section beam to replicate the internal web of a wind turbine blade. They achieved strong numerical and experimental result correlation, but only until the point of adhesive fracture initiation, highlighting possible limitations for this type of analysis in the software package they used. Ji et al. [3], used a fracture mechanics approach to determine the critical stresses and fracture energies of an epoxy adhesive used in wind turbine structures. Using these values, they modelled the adhesive behaviour by implementing a CZM in a different FE software package to that used in [10]. This CZM was validated through numerical and experimental result comparisons with a 3-point-bending end notched specimen with high similarity (within 2%) between FE and experimental results. This validated CZM was then used to investigate adhesive failure of a support web within a full-scale turbine blade under extreme flap-wise bending.

Although some work has been done on investigating adhesive joints in wind turbine blades under general loads, there is a lack of studies investigating adhesive bond behaviour during indentation (or impact) loading conditions. Therefore, the aim of this study is to investigate the behaviour, using FE with CZM, of composite-to-composite adhesive bonds found in large wind turbine blades where blade leading edges are susceptible to exposure to elastic indentation loading conditions.

## 2 Modelling and simulations

### 2.1 Cohesive zone model formulation

In fracture mechanics, a material's resistance to fracture can be expressed in terms of two material constants, its fracture toughness,  $K_c$ , or its critical energy release rate  $G_c$  [11]. A CZM utilises a strength-based fracture criterion to determine failure initiation, along with an energy-based criterion to predict the crack propagation [12]. Before

failure, the bonded surfaces are held together by cohesive traction stresses on which damage initiation is dependant. Following crack initiation, the traction stresses decrease as the surfaces separate and the crack propagates. Generally, the traction–separation law is defined by a variety of relationships such as triangular, exponential and trapezoidal shapes. Using this relationship, the CZM is modelled as linear elastic up until damage of the cohesive elements occur. Upon failure, the material will degrade and behave as defined by the traction–separation law.

Within an FE model the CZM assumes that one or multiple fracture interfaces/regions can be artificially introduced in structures, in which damage growth is allowed by the possible introduction of a discontinuity in the displacement field.

In this study, the interfaces between the two adherend were modelled in ANSYS v.17 using a CZM with interfacial contact as a series of springs whose stiffness varied as a function of the displacement. CONTACT172 and TARGET169 elements with the de-bonding option were created along the interface. The overall behaviour was represented by a triangular traction–separation law to determine the energy release rate during failure propagation as also used in.

The damage initiation and energy criteria as used in [3] and here are defined in Eqs. 1 and 2, providing the necessary theoretical damage and propagation relationships for the CZM. Initial damage criteria are described by:

$$\left(\frac{\sigma^n}{\sigma_{max}^n}\right)^2 + \left(\frac{\sigma^t}{\sigma_{max}^t}\right)^2 + \left(\frac{\sigma^s}{\sigma_{max}^s}\right)^2 = 1 \quad (1)$$

where  $\sigma^n$ ,  $\sigma^t$  and  $\sigma^s$  are the normal, tangential and shear stress components in the adhesive material, respectively. The energy release and crack propagation criteria was defined as:

$$\left(\frac{G_I}{G_{IC}}\right)^n + \left(\frac{G_{II}}{G_{IIC}}\right)^n + \left(\frac{G_{III}}{G_{IIIC}}\right)^n = 1 \quad (2)$$

where  $G_{IC}$ ,  $G_{IIC}$  and  $G_{IIIC}$  are the critical fracture energy release rates in the three fracture modes. It should be noted that in the case of a 2D analysis or where both material shear properties are the same, it is only the first two modes (Mode I and II) that are of significance. The CZM and hence adhesive bond interfaces will not fail under compressive stress [13].

### 2.2 Cohesive zone model validation

The CZM used in this study was validated against the work of Ji et al. [3] who carried out experimental and numerical analysis on two unidirectional glass fibre reinforced

**Fig. 2** **a** Geometry, dimensions and location of supports and facing pin **a** side and **b** end views, **b** boundary conditions and loading of the model employed, and **c** mesh plot of composite-adhesive-composite lay-up (image focussed at joint location to show mesh detail), and bias factor is ratio of the largest edge to the smallest edge

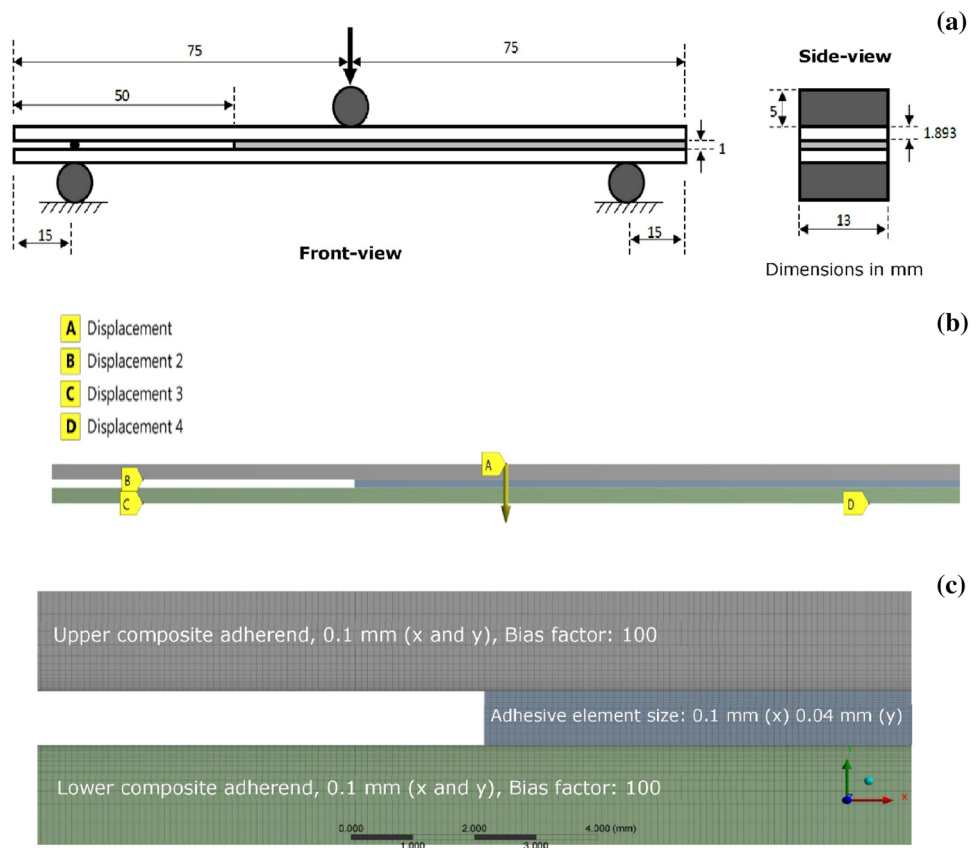


**Table 1** Composite (adherend) properties [3]

Properties	Composite value
Elastic modulus in fibre direction, $E_{11}$ (GPa)	41.4
Elastic modulus transverse to fibre, $E_{22}$ (GPa)	13.56
Tangential elastic modulus (in-plane), $G_{12}$ (GPa)	3.5
Poisson ratio, $\nu_{12}$	0.31

**Table 2** Adhesive and CZM properties [3]

Properties	Adhesive value
Elastic modulus, $E$ (GPa)	4.2
Poisson ratio, $\nu$	0.45
Normal tensile strength, $\sigma_{max}^n$ (GPa)	0.012
Shear (tangential) strength, $\sigma_{max}^t$ (GPa)	0.048
Mode-I critical fracture energy release rate, $G_{IC}$ (kJ/m <sup>2</sup> )	0.4
Mode-II critical fracture energy release rate, $G_{IIC}$ (kJ/m <sup>2</sup> )	0.8

epoxy composite layers (Fig. 2), bonded with a brittle epoxy-based structural adhesive that was applied to the load-carrying components of a wind turbine blade, with relevant mechanical properties listed in Tables 1 and 2.

It is important to note that glass fibre are made of small glass fibers that are connected together to form a material, and the glass is made of silicon and not carbon, whereas, carbon fibre is made with small strands of carbon atoms that are combined into strands woven together to form durable and lightweight single mass material. Glass fibre requires an epoxy to maintain its strength and durability. Without the hard-outer covering, fiberglass is likely to come apart.

The 2D geometry implemented by Ji et al. [3] was replicated for this study using the ‘Static-Structural’ solver in ANSYS® 17.0 and is shown in Fig. 2a. The aim of this validation procedure was to replicate their load–displacement curve and shear stress distribution at failure. Material properties of the composite, adhesive and CZM implemented in the ANSYS® model throughout are show in Tables 1 and 2.

To simplify the model and boundary conditions, the supports and loading pin were not modelled, with displacement boundary conditions being defined to represent the structural set up shown in Fig. 2b. A 5 mm vertically downward displacement was applied to the upper adherend along with a horizontal restriction, while the lower adherend was constrained in the vertical direction. The contact behaviour for the composite-to-adhesive interface was set to ‘bonded’ and followed a pure



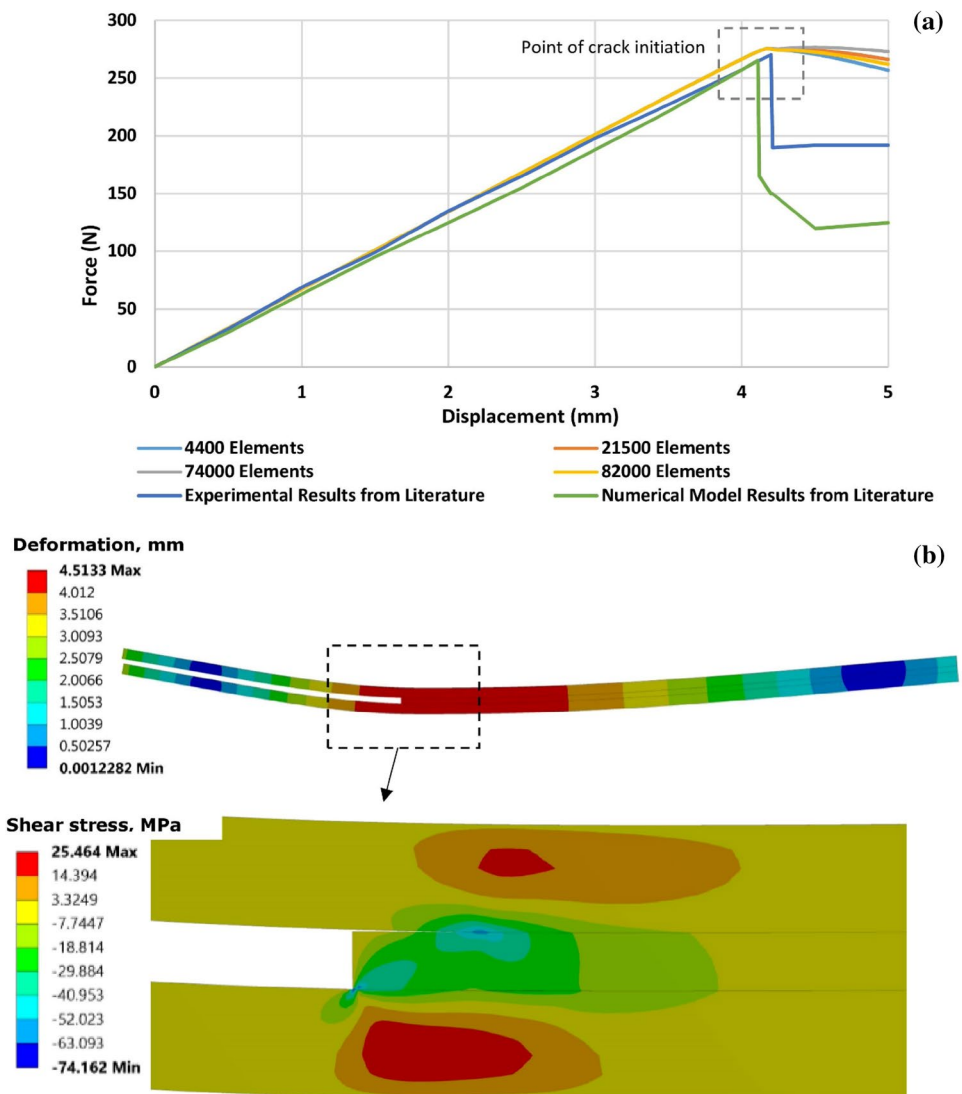
penalty formulation (which introduces a force at the contact detection point(s) which have penetrated the target surface with the express purpose of eliminating the penetration). To implement the CZM and model the fracture mechanics, these bond interfaces were assigned 'contact de-bonding' through the 'fracture' tool. Without defining this behaviour, the bonds in this model would be perfect and never fail.

Meshes were constructed using the automatic meshing capabilities of ANSYS® with a more refined mesh near the adhesive region where large stress gradients were expected and taking advantage of the bias effects, which allowed grading the element size in the adherends from the loading points towards the contact regions, as shown in Fig. 2c. A mesh convergence study was carried out by investigating force values as well as shear stress along the top adhesive-to-composite bond, with satisfactory convergence being achieved.

The numerical results for four different mesh sizes were compared, in Fig. 3a, with both the experimental and numerical results achieved by [3]. As can be seen, the FE model showed a good agreement, within approximately 2% of the experimental results and 3.8% of the numerical results until adhesive failure (the point of crack initiation). This implies that the model adequately predicted the damage initiation and fracture behaviour and hence, the CZM approach can be used to predict failure of adhesively bonded joints.

Deformation and shear stress distributions throughout the structure were used to further compare and validate the FE model. As can be seen in Fig. 3b, the numerical results compare well with those from [3], in which stress distribution and displacement patterns match conclusively. This further confirms that the modelling undertaken in ANSYS® has been successful and can be implemented in further investigations with confidence. This CZM approach

**Fig. 3** Cohesive zone model validation: **a** load–displacement curves for FE model (4 different mesh sizes) along with experimental and numerical results of [3], and **b** deformation and shear stress distribution at critical point where the crack has just begun to propagate



could then be extended to predict the failure in the leading-edge adhesive joints of wind turbine blades.

### 2.3 Leading-edge composite-to-composite adhesive joint model

The proposed methodology and model provide a simplified solution to investigating impact by using an indentation model as an initial step towards understanding the effects of strikes on turbine blades. FE analysis of the leading-edge composite-to-composite adhesive joint in a wind turbine blade was carried out using the validated CZM approach. The geometry investigated in this study was based on the work carried out by Keegan et al. [14], and shown in Fig. 4, and represents the leading-edge geometry of currently manufactured turbine blades. The composite thickness implemented in their study was

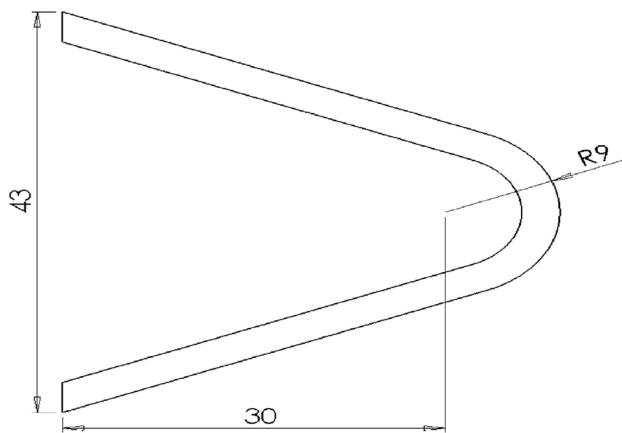


Fig. 4 2D leading edge geometry investigated in this study. (Adapted from Keegan et al. [14])

approximately 2 mm and this thickness was also implemented in this study. Leading edge composite thickness is known to range from 2 to 5 mm near the blade tip. The initial adhesive thickness chosen for analysis was 0.5 mm. Composite (adherend), adhesive and CZM properties from the validation model mentioned above were implemented in this analysis using relevant properties (Tables 1 and 2). An elastic indenter material with properties taken from [14] was selected to imitate ice balls (hailstone) with three different diameters and a square shape (Table 3). Deformation behaviour within the indenter was not part of this analysis. Therefore, this study proposed an indentation (or contact mechanics) based numerical method to investigate the failure of different leading-edge bond configurations exposed to different indenter shapes (spherical representing Hertzian contact and square acting like a flat punch). A numerical model of the specimen was developed using 2D finite element analysis.

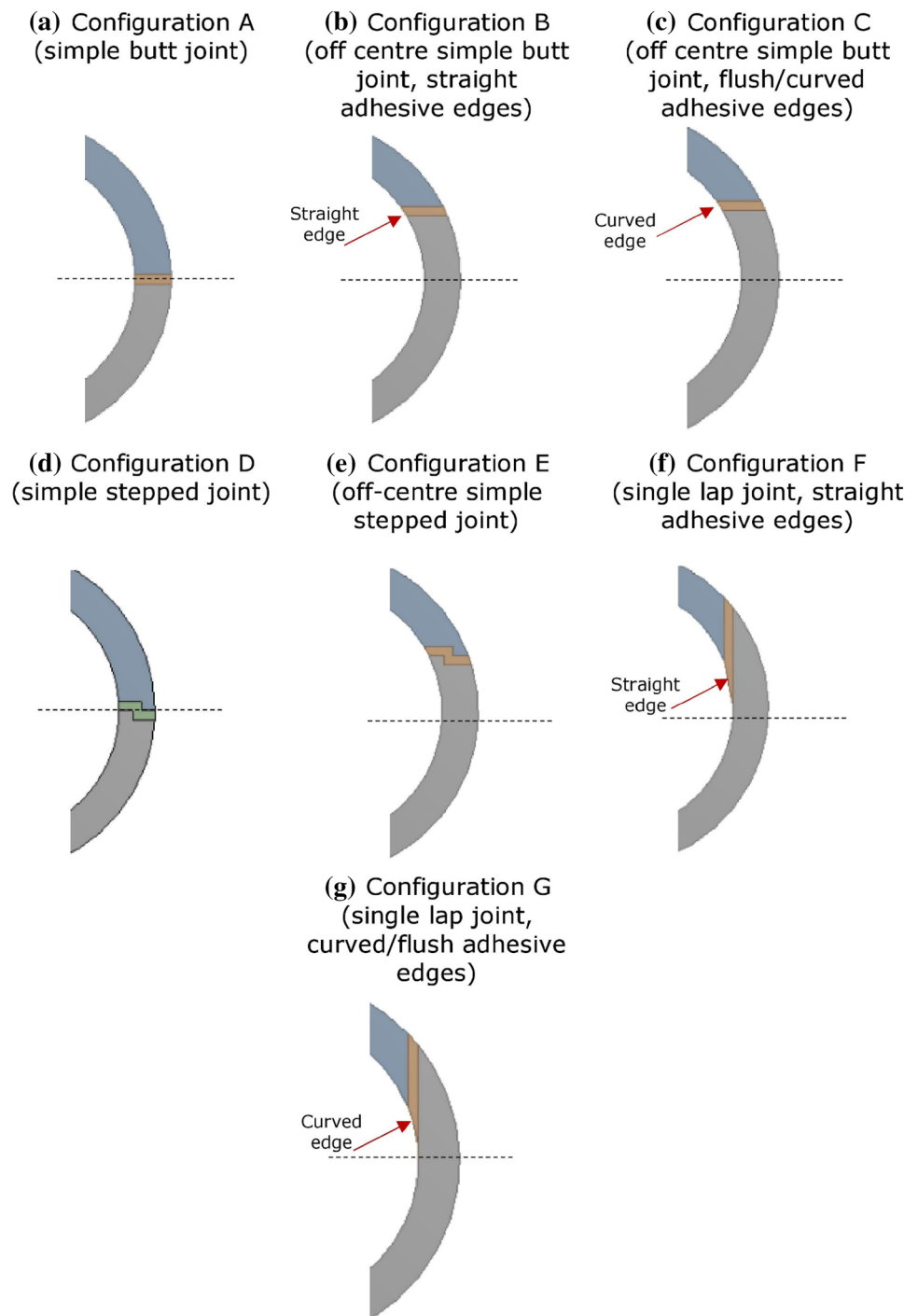
The assumptions made for the model included: (a) simplified geometry represented in 2D, (b) contact mechanics treated as cylindrical to cylindrical contact or cylindrical to flat plate contact, (c) a small region of cylindrical to cylindrical contact, making the 2D assumption valid, (d) plane stress assumed since only a thin slice was represented. It should be noted that the adherend materials were assumed to be orthotropic (in this case, elasticity modulus in fibre direction,  $E_{11} = 41.4$  GPa elasticity modulus transverse to fibre,  $E_{22} = 13.56$  GPa, see Table 1). Also, the adhesive bond interface was perfect i.e. with no manufacturing defects such as dust, bubbles or other impurities in the adhesive or along the adhesive bond lines.

A summary of the leading-edge joint configurations is shown in Fig. 5. These configurations were chosen to allow for factors such as joint positioning, adhesive thickness, adhesive shape and applicability to real wind turbine

Table 3 Finite element method-based crack initiation load and displacements results for all leading-edge joint configurations with 0.5 mm adhesive thickness

Configuration	Indenter	Displacement for crack initiation (mm)	Crack initiation load (N)	Location
A (simple butt)	Spherical (5 mm)	0.212	52.01	Both CZ. Inside edge
A (simple butt)	Spherical (10 mm)	0.212	53.99	Both CZ. Inside edge
A (simple butt)	Spherical (15 mm)	0.212	53.15	Both CZ. Inside edge
A (simple butt)	Square	0.212	55.81	Both CZ. Inside edge
B (off centre simple butt straight)	Square	0.104	91.17	Bottom CZ. Inside edge
C (off centre simple butt curved)	Square	0.102	89.01	Bottom CZ. Inside edge
D (simple centred step)	Square	0.119	39.02	Top CZ. Inside edge
E (off centre simple step)	Square	0.087	69.79	Bottom CZ. Inside edge.
F (single lap straight)	Square	0.955	854.60	Top CZ. Inside edge
G (single lap curved)	Square	1.200	1078.70	Bottom CZ. Internal delamination near inside edge

**Fig. 5** Wind turbine blade leading edge joint configurations (A to G)



blade applications to be investigated. Moreover, straight and curved adhesive body finishes were selected to investigate the effect of an 'ideal' (curved) finish, achieved in practice from moulding, and 'non-ideal' (straight) adhesive edges where the manufacturing process could cause defective and deformed adhesive edges.

The boundary conditions of the proposed model can be seen in Fig. 6a. The two-left-hand side flat edges were fixed with a vertical displacement and a horizontal restriction, as

in practice this geometry would be supported by a shear web or spar cap at these points. Displacement was applied to the indenter in the negative x-direction to simulate the indentation that might occur due to impact or contact with an object. The magnitude of this displacement was varied throughout the analysis. To ensure efficient convergence of each simulation the indenter was displaced only enough to cause crack initiation and the first steps of propagation. Configuration A, with simple butt joints as shown



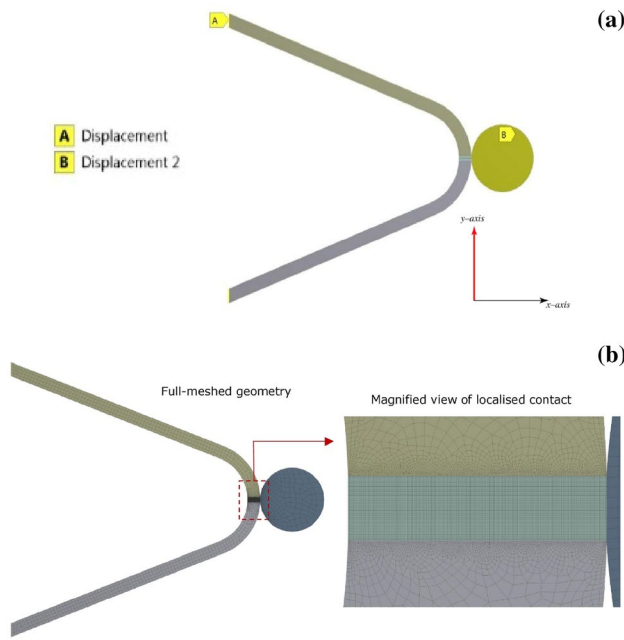


**Fig. 6** Finite element model: **a** boundary conditions and geometry, **b** meshing showing full body meshed geometry, and a magnified view of localised contact (boxed region of left figure)

in Fig. 5a, was selected to carry out the mesh convergence study for the composite body, contact interface and adhesive body. Figure 6b shows the full geometrical model and a refined mesh for the joint A configuration with 10 mm diameter spherical indenter. Adequate convergence was observed with an element size of 0.01 mm at the bond contact interfaces and 0.5 mm throughout the rest of the body, whilst the contact face of the indenter body was given an element size of 0.08 mm. Although other joint configurations have more complex adhesive geometries compared to configuration A, this converged mesh size was maintained at the contact interfaces throughout all the analyses.

The FE method outlined throughout this section was applied to each of the leading-edge joint configurations shown in Fig. 5. Initial analysis was carried out to investigate all of the proposed configurations under indentation contact with the square object to identify crack initiation load and characteristics of failure. Results were extracted using the 'Contact Tool' between the bond interfaces to identify the point and load at which a crack initiated (when the contact status changed from 'sticking' to 'sliding'). Table 3 shows the predicted FE crack initiation load, displacement and crack initiation locations for all joint configurations exposed to the defined indentation cases.

The effect of varying the indenter size and shape was also investigated. Configuration A was chosen for this analysis with all four indenter cases being analysed as shown

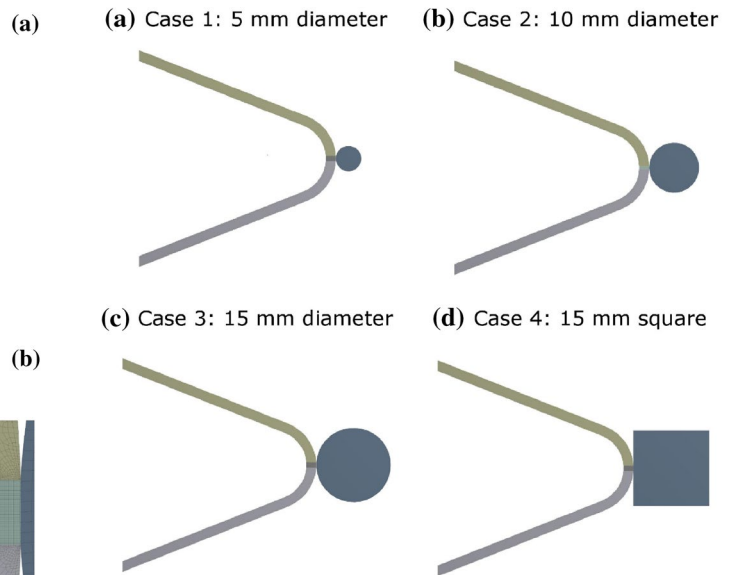


**Fig. 7** Four indenter cases where the indenter size and shape were varied for configuration A

in Fig. 7. This was followed by a detailed stress analysis of the leading-edge adhesive bodies, with stress results at crack initiation being extracted. On completion of this analysis the strongest joint configurations (F and G) were selected for more detailed investigation where variations in adhesive thickness and stress behaviour along the fracture path were analysed.

### 3 Results

#### 3.1 Adhesive joint configuration strength

With reference to the leading-edge joint configurations shown in Fig. 5, Table 3 highlights the key indentation-based FE results that give an indication of the adhesive joint configuration's strength. As can be seen, the least and most resistant joint configuration to adhesive failure were identified. In configuration A, where varying indentation cases were investigated, crack initiation load declined by 4.76% between the most severe (5 mm spherical indenter) and least severe (square indenter) indentation contact. The configuration that possessed the worst strength characteristics was the centred simple step joint (D), with a crack initiation load of 39.02 N. The off-centre simple step joint (E) exhibited the poorest fracture resistance of the off-centre configurations, with a crack initiation load of 69.79 N. The strongest joint configurations were the lap joints, with F predicting a 95.4% and G a 96.4% greater load carrying capability than the weakest joint D. Off-centre joints were shown to be capable of withstanding between 39 and 96%

more load before fracture, compared to the centred joint configurations. For the lap joints, a perfectly curved adhesive finish (G) led to a 20.78% increase in adhesive fracture load, compared to the imperfect straight adhesive edge finish (F). However, the off-centred simple joint for the perfect adhesive edge finish (E) exhibited a 2.37% reduction in fracture load compared to the imperfect straight finish (D).

Figure 8 further illustrates the reduction in fracture strength with decreasing indenter size as shear and normal stresses increased by 74.1%, 70.7% and 38.1% respectively between the most extreme 5 mm indenter case and the square (flat punch) indentation contact.

To analyse the failure of adhesive joints used in wind turbine blades only stresses which contribute to adhesive failure, such as shear stress and normal stress in x-direction and y-direction, were considered in this study. Stress plots for all adhesive configurations were analysed, with the location of the crack initiation highlighted by the circles in Fig. 8. It should be noted that all stress distributions presented are at the time of fracture initiation.

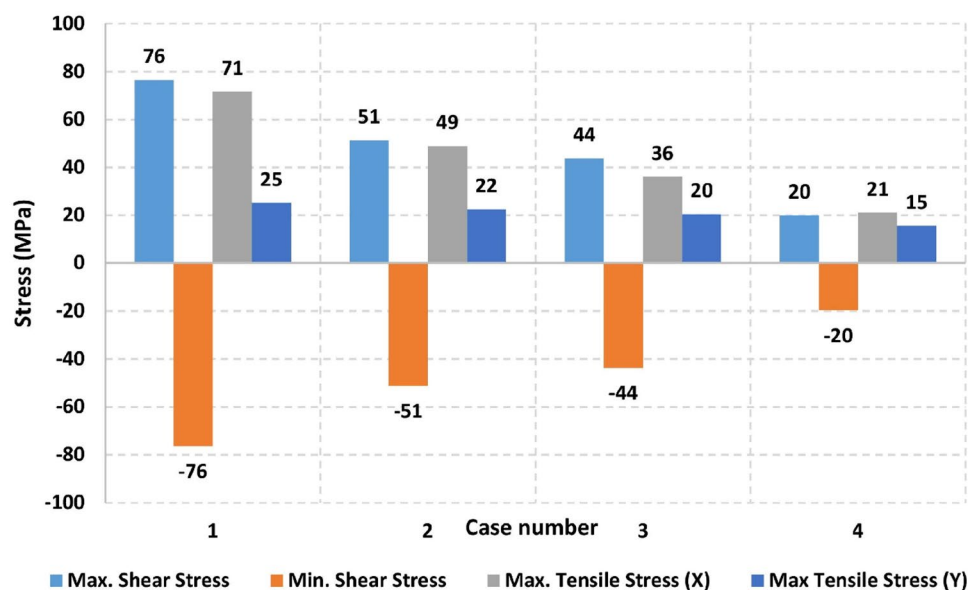
### 3.2 Stress distribution for various configurations

From shear stress plots through the adhesive body (Fig. 9), along with the shear strength values of the adhesive and CZM (Table 2), it can be identified whether or not these stresses are the cause of fracture initiation. In configuration A the areas of shear stress do not coincide with the location of fracture initiation and are well below the adhesive shear stress failure criterion, so are not the cause of failure. In configurations B and C the maximum negative shear stress does coincide with the location of fracture. However, the stress values are significantly lower than the

adhesive shear strength failure criterion of 48 MPa. Again, this suggests that this is not the cause of fracture. In configurations D and E the locations of extreme shear stress concentrations do not coincide with fracture location, suggesting that shear stresses are not the cause of fracture. In configurations F and G, significant areas of negative shear stress, up to 29% greater than the adhesive failure criteria value, coincide with fracture location closely. Shear stress may contribute to mixed mode failure in configurations F and G, but it is not the conclusive cause of fracture. Since there is no definite correlation between shear stress and crack initiation location in the other adhesive bodies, it is difficult to conclude that these stresses contribute to failure.

Figure 10 shows the x-direction normal stresses through the adhesive. It allows the x-direction normal stress to be investigated to determine if this contributes to fracture initiation by coinciding with its location. In configuration A, the location of fracture does not coincide with the maximum tensile stress value. In configurations B and C, areas of maximum tensile stress do coincide with fracture initiation location, but are well below the failure criterion of the adhesive. In configurations A, B and C stresses in this direction act along the bondline interface, hence do not cause Mode-I opening. Configurations D and E exhibit significant areas of tensile stress that are up to seven times larger than the adhesive failure criterion, however these areas do not coincide with fracture initiation locations. In configurations F and G significant compressive stresses exist normal to the adhesive bond line, so do not contribute to fracture initiation. In configurations F and G areas of high tension that are in excess of the adhesives normal failure criterion (12 MPa) exist at crack initiation locations.

**Fig. 8** Variation of stress with different indentation cases shown in Fig. 7



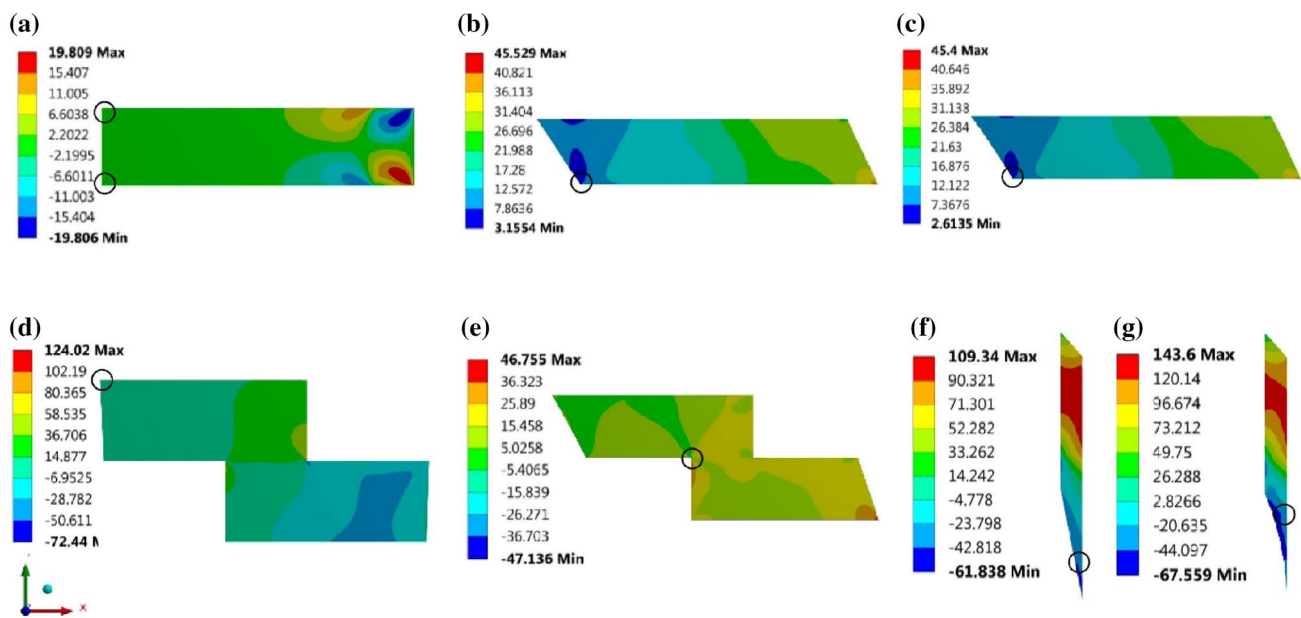


Fig. 9 Local adhesive body shear stress contour plots for configurations A to G (values in MPa). Crack initiation location highlighted with the circles

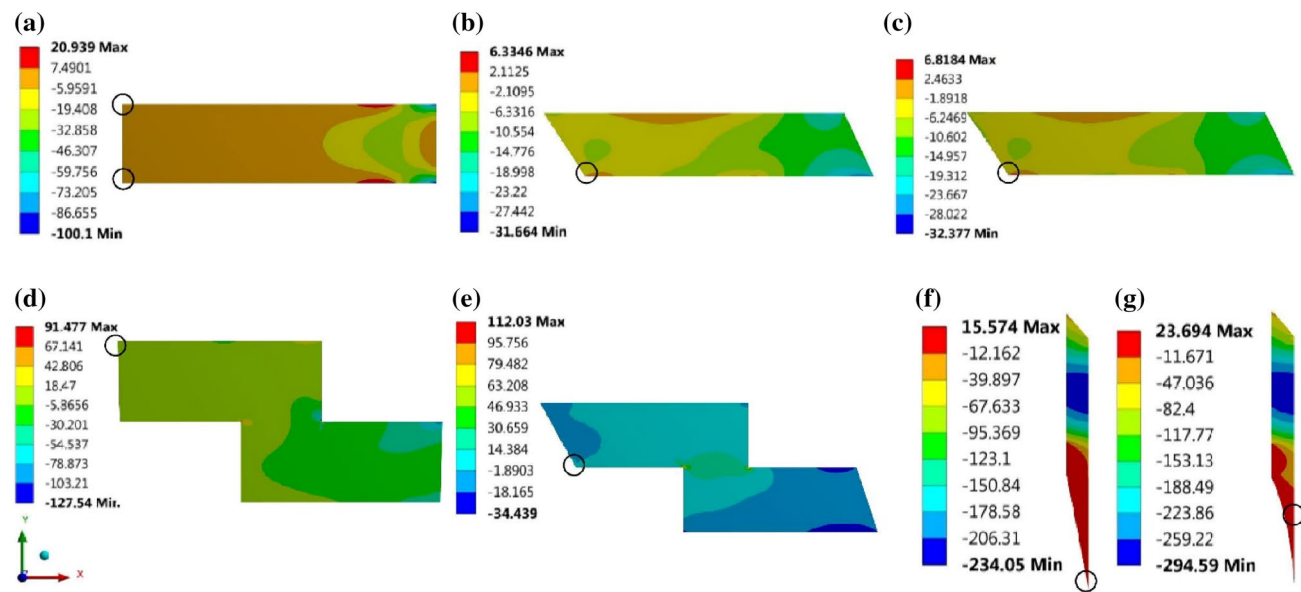


Fig. 10 Local adhesive body normal stress (x-direction) contour plots for configurations A to G (values in MPa)

This indicates that Mode-I failure is likely to be the cause of fracture initiation in configurations F and G.

Figure 11 shows the y-direction normal stresses throughout the adhesive body to allow for relationships between these stresses and fracture initiation to be investigated. In configurations A, B and C stress in this orientation acts normal to the bond line, not along it, hence tensile stresses will cause Mode-I opening to

occur. This is conclusive in configurations A, B, and C as maximum tensile stress coincides with fracture location and exceeds the normal failure criterion of the adhesive (12 MPa). Configurations D and E show an inconclusive relationship between maximum normal stress in this orientation and fracture initiation location. Maximum stress values exceed the failure criterion of the adhesive significantly (by 96.8% in D and 93.15% in E). However,

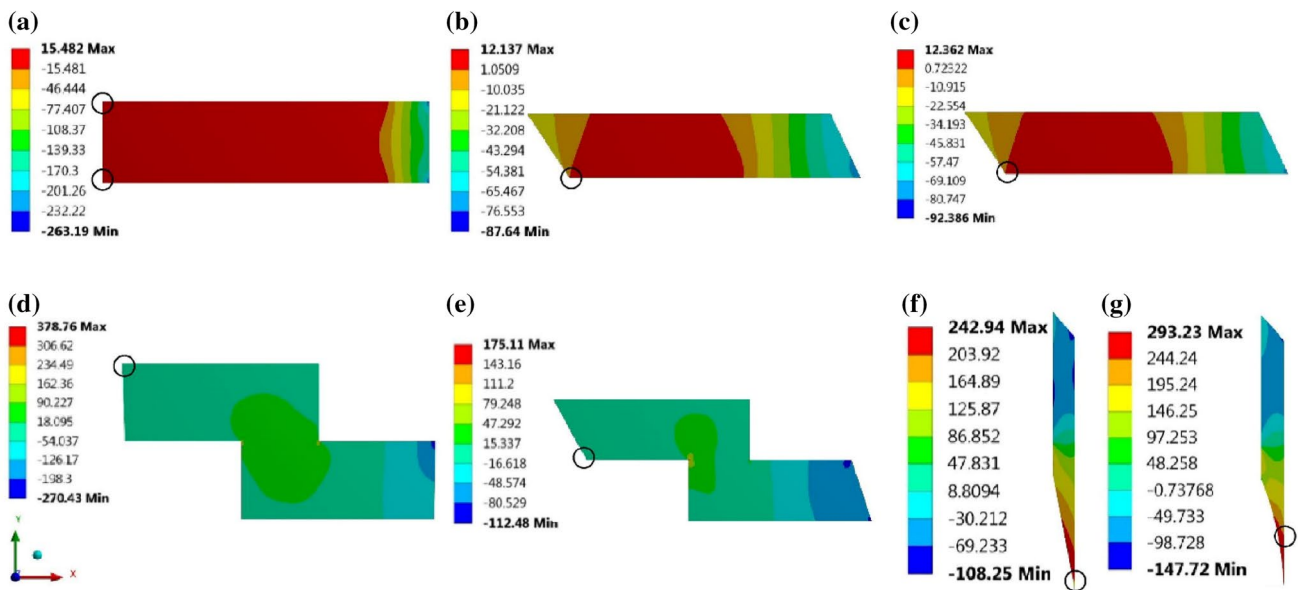


Fig. 11 Local adhesive body normal stress (y-direction) contour plots for configurations A to G (values in MPa)

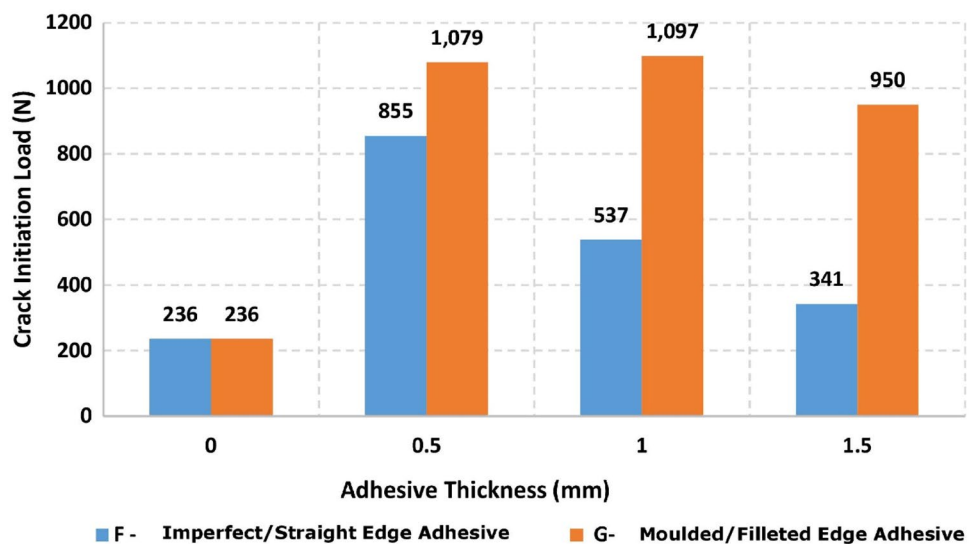
they do not coincide with fracture initiation location. In configurations F and G stresses in this orientation act along the bond line and do not contribute to fracture initiation. Reasons why the adhesive is capable of withstanding stress along the bond interface are discussed later.

As configurations F and G possess superior fracture resistance over other joints investigated, it was decided to investigate these configurations in more detail, including an analysis of the effects of adhesive thickness and fracture behaviour.

### 3.3 Effect of adhesive thickness and crack initiation load

Figure 12 shows the results of adhesive thickness variation on crack initiation load. As can be seen, configuration G with an adhesive thickness of 1 mm is the most resistant to fracture. Thicknesses above and below this value cause a weaker joint, though the 0.5 mm joint is very close in strength to the 1 mm. In configuration F, 1 mm is not the optimum thickness, highlighting that the non-perfect adhesive edge finish effects the load carrying capability of the joint. The pattern of crack initiation load change with bond line thickness agrees with the experimental work

Fig. 12 Effect of adhesive thickness on crack initiation load for joint configurations F and G



carried out by Canales [15] who observed a peak adhesive thickness with reduced strength characteristics above and below the optimum thickness for an epoxy-based adhesive. He concluded that the reason for weakness in the thinner adhesive bond lines was due to an increased strain caused by the inverse relationship between strain and adhesive thickness. In thicker bond lines, the reason for these characteristics in experimental work is due to an increase in voids/defects through a thicker adhesive. In the case of this analysis, this explanation for thick adhesives is not valid as the adhesive is assumed perfect in the FE model. Reasons for a reduction in strength with increasing adhesive thickness can therefore be explained by its reduced tolerance to deformation, due to its brittle characteristic and inability to flex.

### 3.4 Stresses along the adhesive paths

To investigate the fracture behaviour of the failing adhesive edges, stress results were extracted along the failing bond-line at both crack initiation condition (point where detectable crack initiation occurred) and maximum displacement condition (crack fully developed and propagated). Shear stress results along the adhesive path are shown in Fig. 13i-a, b for the crack initiation and maximum displacement conditions respectively. Figure 13ii, iii show similar plots for x-direction normal stress, and for y-direction normal stress, respectively. These results confirm the location of crack initiation as being at the internal adhesive edge corner (0 mm along bond line) in configuration F, and internally (approximately 1.5 mm along the bond line) in configuration G (see Fig. 13iii-a). At crack initiation, significant stress concentrations at the fracture locations are evident, as seen in Fig. 13i-a suggesting that Mode-II failure may in fact contribute to fracture initiation. This is followed by a smooth distribution of stress throughout the remaining bond line. At maximum displacement conditions (Fig. 13i-b), significant shear stress concentrations at the crack tips can be seen.

At crack initiation, there are areas of tensile stress concentrations that coincide with fracture initiation locations, like the trend seen with shear stress. The concentrations of stress are of the order of the tensile failure criteria of the adhesive and confirm that Mode-I opening contributes to fracture initiation. These stress concentrations are also observed at the crack tip as the fracture propagates, with a redistribution of stress along the bond interface past the crack. At crack initiation, there are significant stress concentrations that are much greater than the failure criteria proving that the adhesive is capable of withstanding significant stress along its bond line. Stress concentrations are present at crack tip locations, matching the patterns observed with shear and normal (x-direction) stress. Once

crack initiation has occurred, normal stress concentrations at the crack tip in this orientation may cause Mode-II conditions that contribute to crack propagation.

## 4 Discussion

Each configuration (A to G) was analysed and critically discussed, referring to the presented results to understand the characteristics of adhesive failure.

### 4.1 Joint A (simple butt joint)

This joint proved to have poor fracture resistance, only capable of withstanding a load of 55.8 N (see Table 3, square indenter) before adhesive fracture occurred, and possessed even poorer fracture resistance capabilities in circular indentation cases when contact effects were more significant. This highlighted that the size and shape of indenter can influence the stress distribution, and hence fracture behaviour of the adhesive, with a 4.7% reduction in fracture resistance with decreasing indenter size from 15 to 5 mm diameter. The smallest diameter cylindrical indentation case proved to cause the most significant stress distribution throughout the adhesive, as was shown in Fig. 8, causing 71.4% greater shear stress, 70.7% greater x-direction normal stress and 31.8% greater y-direction stress than a square/flat punch indentation. This behaviour was expected and agrees with contact mechanics theory [11, 16]. The crack initiation location, in Fig. 11a) coincided with the area of highest tensile stress which exceeded the adhesive normal stress failure criterion of 12 MPa (Table 2). This concludes that Mode-I opening is the dominant cause of fracture initiation in this configuration.

Normal stress along the x-axis is not considered the cause of fracture because it acts along the bond line. Where this bond line is still bonded, there is no difference in stress between the adhesive body and the composite body. Without a difference in stress between these two interfaces, there will be no occurrence of fracture initiation conditions. If there was a difference of stress between the two bodies, it is likely to cause Mode-II sliding to occur. Conditions like this would occur after crack initiation, suggesting that Mode-II sliding contributes to crack propagation. This is an important concept to understand and helps explain the behaviour and capabilities of the adhesive bond line to withstand stresses along its interface.

### 4.2 Joint B and C (off-centre simple joints)

Joints B and C proved to exhibit better fracture resistance capabilities than the simple butt joint (A), as they withstood up to 38.8% greater load before fracture initiation.



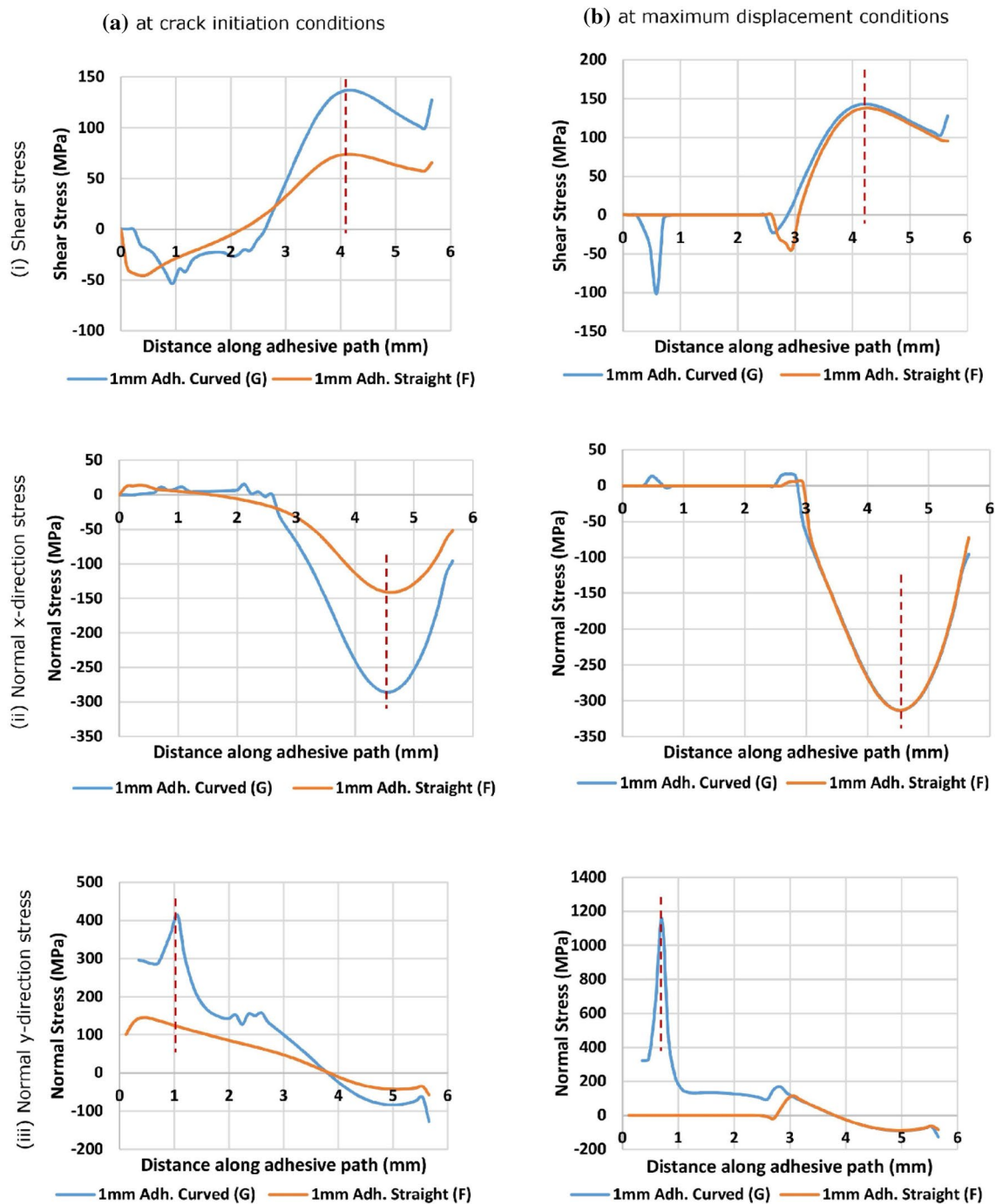


**Fig. 13** Various stresses along the adhesive path of the failing bond line of the adhesive path for configurations F and G (1 mm adhesive) at **a** crack initiation, and **b** maximum displacement (1.35 mm) conditions [dotted line shows some of the peaks in various plots]

This can be explained by considering the distribution of normal stress throughout the adhesive body. As previously highlighted, normal tensile stress in the y-direction (Fig. 11b, c) is extremely high at the centre line of the inside composite edge. The off-centre configuration positions the joint in an area away from this significant stress, hence allowing for greater displacement and force to

be exerted on the leading edge before adhesive failure occurs. Due to the fracture location coinciding with the area of maximum tensile stress in the y-direction as seen in (Fig. 11b, c), Mode-I fracture in this orientation is the dominant cause of adhesive failure.

The effect of straight (B) and curved (C) adhesive edges was also investigated. As can be seen in Table 3 the perfect



moulded edge finish has not caused a significant variation of fracture resistance though it did show a 2.3% reduction in crack initiation load. This implies that the effect of the adhesive edge finish has not provided an improved fracture resistance in this case. This disagrees with the work of Hua et al. [9] who showed that a filleted adhesive edge improved joint strength. The differences exhibited here can be explained by the fact that there is little difference in the edge profiles of these bodies at this small scale.

### 4.3 Joint D and E (stepped joints)

Stepped joints D and E showed the poorest fracture resistance characteristics. D was the weakest joint configuration overall and E exhibited the poorest strength of all the off-centred joints. However, an improved fracture resistance with off-centred joint location is exhibited between joints D and E. Generally, the greater bonded area that both configurations achieve, compared to the simple butt joint, should increase the strength of the adhesive joint [17]. However, the stepped joints investigated in this study have shown low fracture resistance. This might be explained by the clear stress concentrations around the corners of the stepped adhesive bodies in all stress plot results for D and E in Figs. 9, 10 and 11. As the areas of stress do not coincide with the areas of fracture initiation, the identification of the dominant failure mode of these configurations is not clear. High concentrations of stress in these areas suggests that, in practice, plastic behaviour of the adhesive or composite could occur before fracture initiates.

### 4.4 Joint F and G (lap joints)

Joints F and G proved to be the strongest joints, able to withstand a load of 854.6 N and 1078.7 N respectively, over 94% more than the weakest joint (D) (Table 3). This can be partially explained by the capabilities of the adhesive bond to withstand large normal force along its bond interface. Also, as previously highlighted, an adhesive and CZM will not fail under pure compression. To further explain this configuration's capability to withstand high force, its orientation and the transition of stresses from composite to adhesive must be explained. As can be seen in Fig. 11f, g, extreme areas of y-direction tensile stress can be observed. However, the orientation of this joint means these stresses act along the bond interface, which has been shown not to be a contributing factor towards crack initiation. The orientation of stress that will cause Mode-I opening failure is the normal x-direction stress shown in Fig. 10f, g, which was shown to be much less significant than y-direction normal stress. This allowed more leading-edge displacement to take place before the critical adhesive tensile failure stress was reached. Therefore, Mode-I opening failure

due to stress in the x-direction is believed to be the dominant failure mode for configurations F and G.

In the lap joint cases of F and G, adhesive edge finish was shown to be a highly significant factor with the perfectly moulded adhesive edge (G) showing a 20.7% increase in fracture resistance compared to the non-ideal straight edge finish (F) (Table 3). These results showed conclusively that the perfect curved joint (G) allowed more deformation to occur before adhesive failure than the non-ideal straight adhesive edge finish (F). The difference in crack location and initiation load can be explained by several factors. Firstly, the non-ideal adhesive edge in F is less tolerant to the displacement being experienced in that area, due to the extra adhesive thickness and its brittle nature. The more significant cause of earlier failure is due to the stress concentrations that occur at the adhesive tip in the non-ideal bond finish. In a filleted curved finish like G, there are no areas of sharp geometrical non-linearity between the adhesive and composite body, hence less significant areas of stress concentration. Increased stress concentrations at the adhesive tip in F can be seen in Fig. 13i-a, ii-a and are the cause of earlier crack initiation. This was shown in the work of Hua et al. [9] who determined that a non-filleted adhesive finish in an internal shear web adhesive joint reduced the strength by 2.4%, due to increased stress concentrations. In this case, a much more significant reduction of 20.7% in adhesive strength is observed though the same explanation applies.

Figure 13iii-a showed crack initiation and propagation behaviours. It can be seen that configuration G fractures internally along the bond interface, resulting in an internal crack that propagates both up and down the interface. The non-ideal adhesive edge (F), exhibits fracture at the inside edge and propagates upwards along the bond line. At crack initiation conditions, there is an erratic distribution of shear stress around the crack location (Fig. 13iii-a), followed by an increase in stress along the adhesive path. The stress concentrations at the crack tips and redistribution of stress along the bond lines cause the continuous propagation of the crack. This is characteristic of the fracture mechanics expected and follows similar patterns to the results of Ji et al. [3] who also showed significant stress concentrations at crack initiation and crack tip locations, with a redistribution of stress throughout the remaining adhesive bond line. Brittle adhesives, like the epoxy-based adhesive investigated in this study, are known to be sensitive to stress concentrations, as highlighted by Petterson [7], confirming the stress behaviour exhibited in this case is valid and characteristic of brittle adhesive failure.

Considering the possibility of composite adherend failure before adhesive bond failure, it is important to compare the stress contour values with the approximate strength values of the composite. Approximate strength

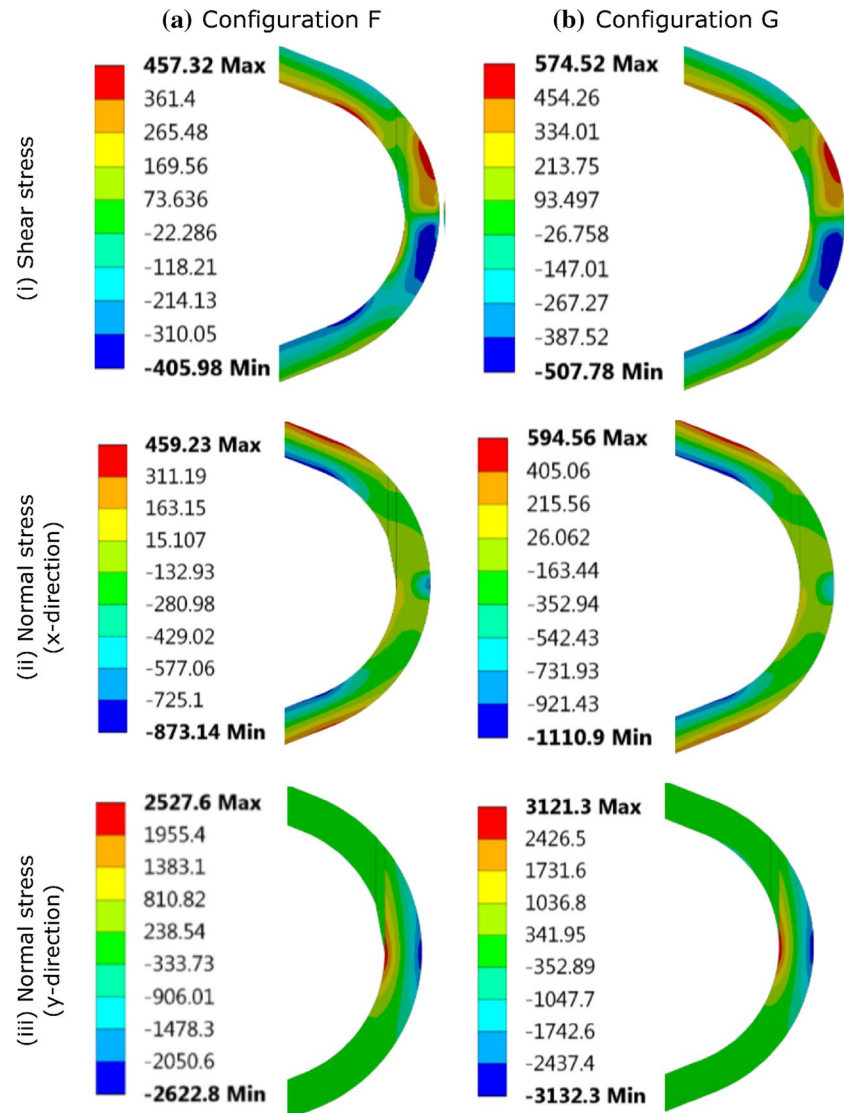
values for glass fibre reinforced epoxy composite extracted from Ref. [18] are (shear strength = 120 MPa; ultimate tensile stress = 410 MPa; compressive strength = 570 MPa). As shown in Fig. 14, global stress contour plots were extracted from the leading-edge body allowing the stress distribution and transition from composite to adhesive to be presented. Lap joints F and G, the strongest joint configurations, all exhibit significantly high shear stress between 74% and 79% greater than ultimate shear strength (as shown in Fig. 14i). This shows that composite failure due to shear stress is extremely likely in these cases. Again, as shown in (as shown in Fig. 14ii, in F and G, excessive tensile and compressive stress that exceed the ultimate strength values of the composite by up to 31% and 49%, respectively, exists at the transition to the curved leading edge. These stresses are caused by the overall deformation of the leading-edge profile as it is indented. And finally, as shown in Fig. 14iii, F and G exhibit normal stresses that

significantly exceed the tensile and compressive ultimate stress values by between 47 to 87% and 42 to 82%, respectively. Extreme areas of tension are located at the internal edge of the leading-edge composite body. Extreme areas of compression are located at the external edge of the leading-edge composite body. These stresses are caused by the overall deformation of the leading-edge profile. As it deforms the curved leading edge is effectively 'straightened out', causing these significant stresses that will cause composite failure.

#### 4.5 Further work

In simple terms, the impact force,  $F_s$ , is given by:  $F_s = \frac{mv^2}{2s}$ , where  $m$  is the mass of an object (kg),  $v$  is the velocity of the object (m/s) and  $s$  is slow down distance (m) that is usually taken as the length of the object.  $F_s$  can be used to estimate the impact force of selected objects and

**Fig. 14** Global leading-edge stress contours for configurations F and G (values in MPa)



hence give an indication of whether the joint configurations investigated can withstand the impact force. If an extreme impact velocity of 120 m/s is considered for possible hailstone impact cases [14], the maximum impact force of a 15 mm diameter hailstone is calculated to be approximately 761 N. This shows that the only configurations capable of being able to withstand this impact would be F and G. It is important to consider how this analysis can develop from considering the static loading indentation cases, to investigating impact. Many materials will behave differently under impact loading, and this is an important phenomenon to understand. Impact loading causes variation in loading phases. These effects are not accounted for in static indentation loading and should be considered in future analysis.

Limitations with the 2D analysis and the effect of the assumptions set out throughout the methodology must be considered. The structure being investigated is 3D in practice, hence simplifying it into a 2D analysis causes potential errors. The plane stress analysis in ANSYS has its limitations as this assumes a thin body. A wind turbine blade is not a thin body with the leading-edge profile being supported by material in the z-direction. The justification for using plane stress is that indentation occurs at a very small localised point along the turbine blade, hence the material along the blade in the z-direction is not affected by the indentation. 3D analysis would produce a much more realistic representation of a leading-edge section exposed to an occurrence of impact. However, time and computational constraints did not allow for the development of such a model. As highlighted by Eder et al. [8] a CZM applied to a 3D model is extremely computationally demanding and rarely implemented in practice, especially where geometrical non-linearity is present, so 2D approximation is needed. They implemented a 2D slice method to analyse a complex leading-edge geometry for investigation using FE, highlighting its success as a model that allowed for high mesh discretisation. This highlights the main justification for proposing a 2D model for the purposes of this study, where geometric non-linearity was present and computational resources were limited.

Due to the ultimate strength of the composite material, plastic behaviour of the composite is extremely likely, making the linear elastic assumption specified for this analysis questionable. Zarouchas et al. [10] confirmed that a linear elastic assumption for the adhesive is acceptable, but a bilinear behaviour is required to accurately model composite failure behaviour. This could not be applied and investigated in this study due to time constraints but should be considered in future investigations. Plastic deformation of a composite body will cause snapping and buckling of composite microfibres if tensile or compressive stresses exceed their ultimate strength value. This would cause damage

propagation throughout the composite body causing significant energy dissipation, reducing the stress on the adhesive bond. Hua et al. [9] proved that considering the effects of plasticity in an FE model of composite to adhesive bonds caused an 8.2% reduction in peel stress (Mode-I), as well as a reduction in shear stress, leading to improved fracture strength. This concluded that in configurations where the strength values of the composite were exceeded, the composite would fail prior to the adhesive, therefore improving the performance of the adhesive. Configurations F and G, are therefore limited by the capability of the composite to withstand leading edge deformation, not by the adhesive joint strength.

In practice, the perfect bond interface assumption is also limited as defects throughout adhesive bodies and their contact interfaces are inevitable. Bubbles through the adhesive or moisture/dust on the contact interfaces are the most likely causes of imperfect bonds. Hua et al. [9] proved that an adhesive body with an elliptical void showed a 4.8% reduction in fracture strength, demonstrating that this is an important consideration to investigate for real life scenarios. These areas of limitation highlight the need for future work and investigation development. However, this study proposed a simplified 2D model that was successful in identifying adhesive joint configurations for development and application to real blade design.

It is likely that the choice in the modification in adhesive joint place and the manufacturing method can restrict the design of the blade and affect the selection of manufacturing materials, quality, performance, and the assembly cost. Other factors influencing the choice in the modification in adhesive joint place are the size and shape of adherend to be bonded, the areas where the adhesive is to be applied, and production volume or rate. The selection of the adhesive joint place and the application of the adhesive bond materials could also depend on the adhesive form (e.g. liquid, paste, powder, film, hot melt, etc.). Importantly, after application of adhesive at the alternative joint places, the assembly must be designed to be mated as quickly as possible to prevent contamination of the bond surface. Also, the substrates will have to be held together under modified pressure and heating conditions, leading to entire curing. The modification in the manufacturing or assembly equipment is also required to perform these functions and which must provide adequate heat and pressure to maintain constant and uniform pressure during the entire curing process.

## 5 Conclusions

In the first investigation of its type, this study presents a simulation method to investigate the structural integrity and failure characteristics of adhesively bonded

composite joint configurations at the leading edge of a wind turbine blade subject to elastic indentation contact. The main conclusions are as follows:

- a. Stepped joint configurations possessed the poorest strength characteristics due to areas of extreme stress concentrations at areas of non-linear geometry. Off-centre joint configurations were capable of withstanding between 39 and 96% more load than centred joints by avoiding areas of high stress and indentation effects. Direct contact with the most severe indentation case on the adhesive body caused up to a 4.7% reduction in load carrying capabilities. This concludes that direct indenter to adhesive contact should be avoided by positioning the joint away from a centred location. Lap joint configurations were the strongest joints, capable of withstanding up to 96.4% greater load before failure.
- b. Mode-I opening was the dominant cause of fracture in joints A, B, C, F and G, with fracture initiation locations coinciding with areas of tensile stress in the order of the adhesive failure criterion. Mode-II was concluded to contribute to crack propagation but was not the dominant mode of fracture initiation. Adhesive characteristics proved that the epoxy-based adhesive was capable of withstanding significant stress along its bond line interfaces, and did not fail under compressive stresses, agreeing with CZM theory.
- c. In the strongest configurations, there were stresses above the strength values (shear strength, ultimate tensile stress, compressive strength) of glass fibre reinforced epoxy composites, suggesting that there would be the possibility of composite failure before adhesive bond failure (e.g. in F and G).
- d. A non-ideal adhesive lap joint finish shows a reduction in resistance to fracture of 20.77% due to high stress concentrations at the transition from composite to adhesive caused by the geometric non-linearity of the straight adhesive edge. This concludes that a perfectly moulded and filleted adhesive edge is recommended for improved adhesive joint integrity.
- e. Finally, it was concluded that a lap joint configuration with 1 mm thick adhesive and a perfectly moulded adhesive finish (G), possessed the best fracture resistance, and would be capable of withstanding extreme impact cases. It was shown that this joint configuration possessed greater adhesive fracture strength characteristics and can be recommended as a joint configuration that justifies further development for application in wind turbine (for a reliable renewable energy production).

**Acknowledgements** The authors are very grateful to the reviewers for their careful and meticulous reading of the paper and providing important feedback or comments, and we would like to kindly acknowledge them.

### Compliance with ethical standards

**Conflict of interest** The authors declare that they have no conflict of interest.

**Open Access** This article is distributed under the terms of the Creative Commons Attribution 4.0 International License (<http://creativecommons.org/licenses/by/4.0/>), which permits unrestricted use, distribution, and reproduction in any medium, provided you give appropriate credit to the original author(s) and the source, provide a link to the Creative Commons license, and indicate if changes were made.

### References

1. Wind Energy Update, End of Warranty Wind Farm O&M Options Report (2012) <http://www.windenergyupdate.com/end-of-warranty/>. Accessed Mar 2017
2. Feraren P, Jensen H (2004) Cohesive zone modelling of interface fracture near flaws in adhesive joints. *Eng Fract Mech* 71:2125–2142
3. Ji Y, Han K (2014) Fracture mechanics approach for failure of adhesive joints in wind turbine blades. *Renew Energy* 65:23–28
4. Floros I, Tserpes K, Löbel T (2015) Mode-I, mode-II and mixed-mode I+ II fracture behaviour of composite bonded joints: experimental characterization and numerical simulation. *Compos B Eng* 78:459–468
5. Hazimeh R, Challita G, Khalil K, Othman R (2015) Finite element analysis of adhesively bonded composite joints subjected to impact loadings. *Int J Adhes Adhes* 56:24–31
6. Prathuru AK, Faisal NH, Jihan S, Steel JA, Njuguna J (2017) Stress analysis at the interface of metal-to-metal adhesively bonded joints subjected to 4-point bending: finite element method. *J Adhes* 93:855–878
7. Petterson J (2016) Analysis and design of an adhesive joint in wind turbine blades. Lund University 2016. <https://www.byggmek.lth.se/fileadmin/byggnadsmekanik/publications/tvsm5000/web5217.pdf>. Accessed Mar 2017
8. Eder M, Bitsche R, Belloni F (2015) Effects of geometric non-linearity on energy release rates in a realistic wind turbine blade cross section. *Compos Struct* 132:1075–1084
9. Hua Y, Kasavajhala A, Gu L (2013) Elastic–plastic analysis and strength evaluation of adhesive joints in wind turbine blades. *Compos B Eng* 44:650–656
10. Zarouchas D, Makris A, Sayer F, Van Hemelrijck D, Van Wingerde A (2012) Investigations on the mechanical behaviour of a wind rotor blade subcomponent. *Compos B Eng* 43:647–654
11. Sun C, Jin Z (2012) Fracture mechanics, 1st edn. Academic Press, Waltham
12. Li S, Thouless M, Waas A, Schroeder J, Zavattieri P (2005) Use of a cohesive-zone model to analyze the fracture of a fiber-reinforced polymer–matrix composite. *Compos Sci Technol* 65:537–549
13. Silva L, Campilho R (2012) Advances in numerical modelling of adhesive joints, 1st edn. Springer, Berlin

14. Keegan M, Nash D, Stack M (2013) Numerical modelling of hailstone impact on the leading edge of a wind turbine blade. <http://strathprints.strath.ac.uk/42830/>. Accessed Nov 2016
15. Canales AG (2008) Evaluation of bondline thickness on wind turbine blade subcomponents. Dissertation, Technische Universiteit Eindhoven
16. Faisal NH, Ahmed R, Reuben RL (2011) Indentation testing and its acoustic emission response: applications and emerging trends. *Int Mater Rev* 56:98–142
17. Hartshorn R (1986) *Structural adhesives*, 1st edn. Springer, Boston
18. Asi O (2008) Mechanical properties of glass-fiber reinforced epoxy composites filled with Al<sub>2</sub>O<sub>3</sub> particles. *J Reinf Plast Compos* 28:2861–2867

**Publisher's Note** Springer Nature remains neutral with regard to jurisdictional claims in published maps and institutional affiliations.